ResearchGate

See discussions, stats, and author profiles for this publication at: https://www.researchgate.net/publication/251503126

The multi-scale physical and numerical modeling of fracture phenomena in the MgCa0.8 alloy

Article *in* Computers & Structures · June 2011

DOI: 10.1016/j.compstruc.2011.01.003

CITATIONS
30

READS
205

3 authors:

Andrij Milenin
AGH University of Krakow
174 PUBLICATIONS **1,159** CITATIONS
SEE PROFILE

Dorota Joanna Byrska-Wójcik
AGH University of Krakow
25 PUBLICATIONS **198** CITATIONS
SEE PROFILE

Olexandr Grydin
Paderborn University
159 PUBLICATIONS **1,139** CITATIONS
SEE PROFILE

All content following this page was uploaded by Andrij Milenin on 08 November 2020.

The user has requested enhancement of the downloaded file.

Computers and Structures xxx (2011) xxx–xxx

Contents lists available at ScienceDirect

Computers and Structures

journal homepage: www.elsevier.com/locate/compstruc

The multi-scale physical and numerical modeling of fracture phenomena in the MgCa0.8 alloy

A. Milenin [a], D.J. Byrska [a,*], O. Grydin [b]

[a] Faculty of Metal Engineering and Industrial Computer Science, AGH University of Science and Technology, Al. Mickiewicza 30, 30-059, Krakow, Poland
[b] Institute of Materials Science, Leibniz Universität Hannover, An der Universität 2, 30823 Garbsen, Germany

ARTICLE INFO

Article history:
Received 5 June 2010
Accepted 10 January 2011
Available online xxxx

Keywords:
MgCa0.8 alloy
Boundary element method (BEM)
Fracture model
Drawing process

ABSTRACT

The MgCa0.8 alloy can be used to produce surgical threads. However, the low plasticity of this alloy causes problems during wire drawing. A numerical model of the drawing process can be used to optimize the deformation parameters. Research has shown that fractures in MgCa0.8 start within grain boundaries; therefore, a model of the drawing process should consider this mechanism. The main purpose of this work is to develop a micro-scale numerical model of fracture in MgCa0.8 using the boundary element method (BEM). Additionally, the potential for using the developed BEM model as a part of the multi-scale model of the drawing process is investigated.

© 2011 Elsevier Ltd. All rights reserved.

1. Introduction

Magnesium alloys with high bio-compatibility have medical applications because of their high compatibility and solubility in the human body [1–2]. The production of surgical threads by wire drawing is an example of an application of these types of materials, which act as alternatives to bio-inert materials such as titanium, tantalum or 316L steel. Corrosion research performed on Mg alloys in vivo showed the possibility for implant solubility, which could eliminate the need for implant extraction [3]. Some promising properties of the MgCa0.8 alloy with respect to these applications include its strength and biological stability, which make it suitable for a long-term implantation and are the focus of interest in [3]. However, the magnesium alloys have low plasticity during cold deformation; therefore, the drawing of thin wires is difficult [4,5].

New technology for the production of tubes and wires from Mg alloys at high temperatures has been described [6–7]. However, after multi-pass drawing of a wire using this technology, multi-stage cold drawing is necessary to improve the surface quality and mechanical properties of the wire. To support this investigation, a numerical model of cold wire drawing is required. A prediction of wire fracture during the drawing of MgCa0.8 alloy is very important from theoretical and practical points of view.

The experiments conducted in [8] showed that the fracture in the MgCa0.8 alloy starts at the grain boundaries and propagates along them. Consequently, the model of wire drawing should include a model of fracture at the micro-scale. Macro-scale fracture models are not able to predict important phenomena, such as cracking along the grains boundaries, the moment of initiation of micro-cracks, stress relaxation in the grain after micro-cracking, etc. Thus, analysis of the fracture phenomena at the macro-scale is not sufficient, and a model targeting the micro-scale is necessary.

The solution to the problem of multi-stage deformation in the MgCa0.8 alloy is connected with the solutions for the following problems.

1.1. The development of a method of experimental studies of fracture on the micro-scale during multi-stage plastic deformation

This method should make it possible not only to observe the process of fracture in the selected fragment of the microstructure at a given time but also to consider annealing in the process of the experiment. This approach should provide the opportunity to determine the optimum state of the metal in the process of deformation at a single stage of deformation. The optimum state should be determined from the condition of the maximum total deformation of the material by determining the parameters of annealing and deformation. Most of the existing work on material failure is based on experiments executed at the macro-level [4,9–11]. An example of the use of experimental data at the micro-level has been reported [12], in which the fracture of the zircaloy-4 was examined. The results of the experiment at the micro-level [12] are used for substantiating the choice of the fracture simulation method. Determination of the empirical parameters of the fracture

* Corresponding author.
E-mail addresses: milenin@agh.edu.pl (A. Milenin), byrska@agh.edu.pl (D.J. Byrska), grydin@iw.uni-hannover.de (O. Grydin).

0045-7949/$ - see front matter © 2011 Elsevier Ltd. All rights reserved.
doi:10.1016/j.compstruc.2011.01.003

Please cite this article in press as: Milenin A et al. The multi-scale physical and numerical modeling of fracture phenomena in the MgCa0.8 alloy. Comput Struct (2011), doi:10.1016/j.compstruc.2011.01.003

model is carried out on the basis of the analysis of micro-cavities at the grain boundaries, which appear during the final stage of deformation. The use of data from only one stage of deformation limits the authenticity of the model because it is not possible to compare the results of the calculation with the other stages of deformation of the same fragment of the microstructure. Attempts to discern a solution to this problem has been reported [8,13,14]. In these works, the procedure for an experimental study of deformation at the micro-level is described, which makes it possible to observe the process of fracture of a selected fragment of the microstructure at the different stages of deformation. The method is based on placing the sample under a special micro-camera and performing the tension in the vacuum chamber of a scanning electronic microscope (SEM). This procedure does not permit annealing at the selected stage of deformation. Because wire drawing is a multistage deformation process with intermediate annealing, the procedure described was developed in the present work.

1.2. The development of a mathematical model of fracture at the micro-scale

First of all, the model should be limited to simulating those phenomena that are observed in the experiment. For example, it is known that the cracks originate at the grain boundaries. Consequently, only this mechanism is relevant from a practical point of view. The existing works in the area of multi-scale simulation are extensively presented in connection with the finite element method (FEM) [8,15–17], extended/generalized finite element methods (XFEM, GFEM) [18–23], smoothed finite element method (SFEM) [24–26], alpha finite element method (FEM) [27] and also with meshless methods [28–32]. In spite of the high mathematical level of these works, the practical applications of these methods as solutions to the problems presented in this work are limited, or even unfeasible, for the following reasons:

- In the overwhelming majority of the enumerated works, material failure is examined from the general prerequisites; however, in this case there is no reason to simulate all the possible mechanisms of fracture.
- Obtaining the empirical parameters of the existing models for the real materials is hindered by the absence of the corresponding experimental procedures.
- A significant amount of time is necessary to obtain a numerical solution, a process that is complicated a priori due to the procedure of identification and requires numerous calculations.

From this point of view, a particularly important work [12] examined a model of fracture along the grains boundaries depending on the stress state in a particular location. The FEM was used in this work for the simulation of the deformation of a fragment of the microstructure. Thus, the solution was determined not only at the boundary but also in the entire volume of grains. In the case examined in the present work, the solution in the entire volume of grains does not have practical importance and leads to a substantial increase in the calculation time.

The problems mentioned above can be solved using the boundary element method (BEM) for simulating the deformation of a representative volume element (RVE). The possibility of solving such types of tasks with the aid of the BEM is described in many publications [33–35].

A method of BEM simulation for the deformation of materials that consist of two phases with different mechanical properties was proposed [36]. The selection of BEM for the development of a micro-scale model has significant advantages over existing FEM models, particularly in the precision of the calculations at the grain boundaries; this advantage occurs because normal and shear stresses, as well as displacements, are calculated directly at the boundaries. In the model described, each grain of the microstructure is treated as a separate zone connected to the neighboring grains only by the boundary conditions, which allows the breakage of the boundaries between grains by simply modifying the boundary conditions. Remeshing is not necessary in that case. This approach to the problem corresponds entirely to the actual mechanism of fracture; namely, cracking along the grain boundaries. Moreover, the great advantage of this model based on BEM is that it significantly reduces the number of variables and enables the analysis of a large number of grains in the RVE. The computational cost in this case is very important because taking into account a greater number of grains makes the results more reliable.

Some essential difficulties appear, however, with the determination of the parameters of such a model and its application to real technological problems.

To solve this problem, a procedure for the identification a model according to the results of experiments at the micro-scale should be proposed together with the mathematical model of fracture. The procedure for model identification can be based on the concept of the inverse analysis, which is well described [37]. The model of metal deformation at the micro-scale is the essential part of this algorithm.

1.3. Implementing the model of deformation at the micro-scale in the macro-scale model of the wire drawing process

In this work, an FEM program [38] is used for the macro-scale wire drawing simulation.

The purpose of this work is to develop a new mathematical model of MgCa0.8 fracture phenomena at the micro-scale on the basis of the boundary elements method. The proposed BEM model at the micro-scale is coupled with the authors' FEM code, which is dedicated to modeling the wire drawing processes at the macro-scale. The wire drawing model that has been developed can be used to optimize the parameters of the drawing process and to predict the ductility of the material.

2. Methodology

The outline of the applied procedure is briefly described as follows:

(1) Experimental studies: Tensile tests are the sources of data for the yield stress model of the MgCa0.8 alloy at the macro-scale.
(2) Experimental studies: In-situ metallographic analysis of the material used for the micro-scale fracture model and analysis of the MgCa0.8 magnesium alloy in a micro-chamber with a 10 kN Tensile/Compression SEM Stage were performed to understand the fracture mechanism. This analysis showed the material was cracking at the grain boundaries. Experimentation in the micro-chamber allows for the determination of the empirical coefficients of the micro-scale fracture model.
(3) Experimental studies: Metallographic analysis of the material during two deformation stages with an intermediate annealing showed the state that precedes the appearance of microscopic cracks at the grain boundaries is the optimum state of the metal after deformation but prior to the annealing. The experimental variable was the deformation after the first step of tension. The state of the metal after the first stage of deformation (the objective function), which corresponds to the maximum of stress, is designated as the optimum state. This state of the metal corresponds to the

Please cite this article in press as: Milenin A et al. The multi-scale physical and numerical modeling of fracture phenomena in the MgCa0.8 alloy. Comput Struct (2011), doi:10.1016/j.compstruc.2011.01.003

most effective use of annealing for restoring the plasticity after the plastic metal forming. The prediction of this state for wire drawing requires the application of the multi-scale model.

(4) The development of the multi-scale numerical model of fracture is assisted by the BEM, which is used for the micro-scale model. A mathematical model of fracture is proposed in the two dimensional domains. The elastic-plastic theory of plasticity is applied. An inverse analysis is used for determining the empirical parameters of the micro-scale fracture model. The goal function is defined as the difference between the measured and the predicted moment of crack initiation and the history of crack propagation at the micro-scale.

(5) The proposed BEM model at the micro-scale is implemented in the authors' FEM code, which is dedicated to the macro-scale modeling of wire drawing. The computer program that has been developed enables predictions and observations of discontinuity along the grains' boundaries during deformation. The relationship between the technological parameters of drawing and the fracture phenomena is obtained using the multi-scale model that has been developed.

3. Experimental procedure

3.1. Development of the yield stress model at the macro-scale

A series of tensile tests were performed at the AGH University of Science and Technology, using a Zwick 250 tensile tester to generate the stress-strain curves of the MgCa0.8 (Mg 99.15%, Si 0.18, Ca 0.67%) alloy. The sample had a 5 mm diameter and a 20 mm deformable base (Fig. 1(a)). Deformation was carried out at room temperature, and the crosshead velocity was 0.16 mm/s. During the experiment, the load and displacement of the crossheads were measured. The experimental results showed that the stress-strain curve is divided into two regions: a non-linear elastic zone and a plastic zone. The transition point between the elastic and plastic zones of the material model is clearly distinguished ($\varepsilon_p = 0.0076$, $\sigma_p = 173$ MPa). The following equation was used as the material model for the examined alloy:

$$\sigma_i = A\varepsilon_i^{n_1} \exp(n_2\varepsilon_i), \quad (1)$$

where σ_i is the equivalent stress, ε_i is the equivalent strain, and A, n_1, and n_2 are the empirical coefficients.

An approximation of the two zones was applied for the model of stress-strain curve. The coefficients of equation (1) were calculated for the elastic and plastic zones, respectively by using the results of the tensile test. The parameters of the stress-strain curve are shown in Table 1. Examples of the stress-strain curve obtained from equation (1) are shown in Fig. 1(b).

3.2. In-situ metallographic analysis of micro-scale fracture

To consider the fracture phenomena in the MgCa0.8 alloy, a second set of experiments were performed at the Institute of Materials Science, Leibniz Universität Hannover using a 10 kN tensile/compression stage for SEM (Kammrath and Weiss GmbH, Fig. 2(a)). The test was carried out in a LEO 1455VP SEM (Fa. Zeiss). A sample used for the in-situ tensile test is depicted in Fig. 2(b). A description of the experimental procedure for microstructural analysis during deformation in the SEM by the tensile/compression stage and the related technical data are described in detail elsewhere [8,13,14].

This procedure enables the observation of the chosen fragment of the microstructure in the process of deformation and the material failure. This experimental approach in comparison with other in-situ methods allows for the direct identification of the crack-formation site, such as grain boundaries or inclusions etc. Due to the high resolution of the SEM, it is possible to detect a microstructure element with a size above 0.5 μm. A fragment of the microstructure that is located in the center of the sample on its axis of symmetry was selected for the analysis. Thus, during symmetrical tensile loading, the selected point does not move noticeably. Technically, to take an image of the microstructure, the tensile loading must be paused without removing the load, after which tensile loading continues until the next image is taken. In this case, the sample is continuously in the vacuum chamber, and the selected fragment of microstructure does not fall outside of the field of observation. The heating element (position 2 in Fig. 2), which enables the physical simulation of annealing in between the deformation stages is the next part of the experimental procedure.

The procedure described does not allow the direct determination of the orientation of grains in the polycrystal; therefore, this factor was not considered in the calculations. However, the authors have performed preliminary studies in this area, and those results will be presented in a separate publication.

During the experiment, the tensile load and deformation (displacement of crossheads) were measured. Three variants of the experiment were carried out (Table 2).

In variant 1, the tensile testing with a crosshead speed of 0.005 mm/s was performed until the sample ruptured. The SEM micrographs were taken at intervals of 0.1 mm of crosshead displacement. In variants 2 and 3, two-step deformation with intermediate annealing was performed. The annealing temperature was 300 °C for 6 min. The heating device on the tensile/compression stage allows the sample to be heated and to hold the temperature

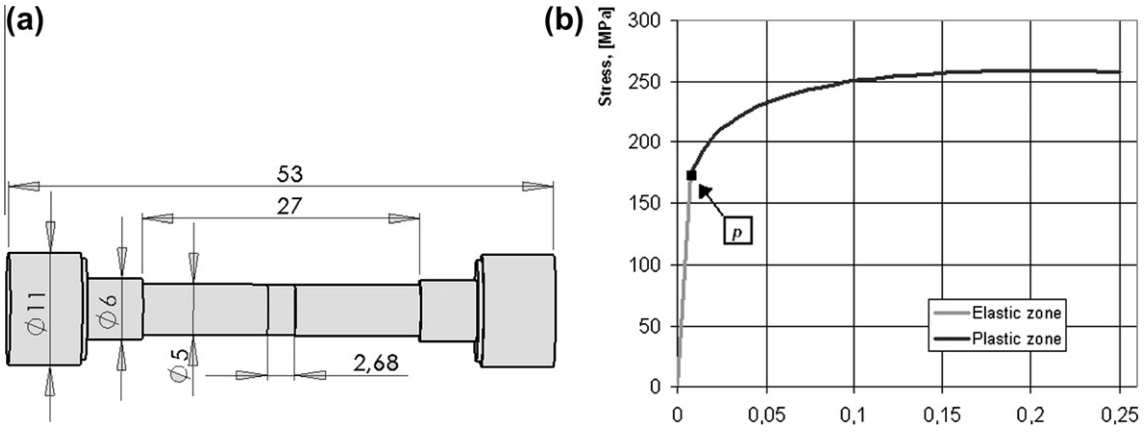

Fig. 1. (a) The dimensions of the sample used for the tensile test and (b) the stress-strain curve for MgCa0.8 alloy, where p is the transition point.

Please cite this article in press as: Milenin A et al. The multi-scale physical and numerical modeling of fracture phenomena in the MgCa0.8 alloy. Comput Struct (2011), doi:10.1016/j.compstruc.2011.01.003

Table 1
Parameters of the stress-strain curve for the MgCa0.8 alloy.

Elastic zone		Plastic zone	
A	12039.68	A	400.2311
n_1	0.776996	n_1	0.168096
n_2	−57.7732	n_2	−0.83199

Table 2
Conditions and results of the experiments in the micro-chamber.

Nr	Deformation between annealing (mm)	Overall deformation, (mm)
1	–	1.49
2	0.8	1.52
3	0.4	1.80

at certain intervals from 20 to 950 °C. However, only the temperature of the heating device plate is measured, and this measurement is used to control the test temperature. To determine the sample temperature, a specimen of the MgCa0.8 alloy with a shape identical to that of the tensile sample (Fig. 2(b)) was prepared with a hole on a flange in the middle of the specimen with a depth of 1.5 mm and a diameter of 0.5 mm. A thermocouple 0.5 mm thick was inserted in the hole. Then, the sample was heated in the SEM chamber to 300 °C, and the parameters of the heating device, such as power and time, were determined. This monitored control procedure was applied to the annealing of the sample. Because the temperature of the material rose during heating, the pressure in the SEM chamber increased too. For this reason, it was impossible to take SEM micrographs during heat treatment of the metal. The crosshead rate for experiments 2 and 3 was 0.005 mm/s.

The deformation at the first step was the varying parameter for experiments 2 and 3. This value was selected on the basis of the microstructural analysis in experiment 1. In variant 1, the sample ruptured after a crosshead displacement of 1.49 mm. The microstructures in the center of sample after different load intervals for this test are shown in Fig. 3. The experiment showed that fracture in the MgCa0.8 alloy starts at the grains boundaries and, as a consequence, it propagates along these boundaries.

The dependence of the sample porosity on the value of deformation is built on the basis of the observed microstructures. The degree to which the sample is deformed without the appearance of porosity is a meaningful result. This value is equal to 0.4 mm (Fig. 4(a)). Another characteristic point on the curve in Fig. 4(a) corresponds to a deformation (displacement) 1 mm. After this point, the porosity increased sharply. This point corresponds to the maximum value of load versus displacement (Fig. 4(b)).

The value of deformation after the first step was selected as 0.8 mm for variant 2 and 0.4 mm for variant 3. The total deformation before the fracture was the goal of the experiment. The maximum value obtained for experiment 3 was 1.8 mm. This allows for annealing before the appearance of microscopic cracks at the grain boundaries. Finally, the prediction of this phenomenon for various conditions of deformation (for example, during drawing) is a very important task. To solve this problem, a numerical model of fracture phenomena at grain boundaries is required. The boundary element method was used to construct a numerical model of cracking at the microstructural level.

4. Multi-scale model of fracture

4.1. Model of fracture phenomena at the micro-scale

There are two important conclusions that follow from the previous discussion and that allow for substantial simplification of the mathematical model of the RVE:

1. The fracture of the material occurs at the grain boundaries only. Thus, there is no need to examine other fracture mechanisms in the model.
2. The optimum state of the metal specific to the experiment corresponds to the moment just before the appearance of microscopic cracks on the grain boundaries. This makes the calculation of the crack development optional from the practical point of view. The calculation of the crack development was executed only for the purpose of obtaining more information for the identification of the model. The calculations of the crack development are interesting from a scientific point of view because they explain the mechanism of reduction in the plasticity in experiment 2, for example (Table 2).

The proposed BEM algorithm is based on the following concept.

The location of the RVE corresponds to the position of the fragment of the microstructure in the sample, in the experimental studies described above.

During the implementation of the obtained micro-model in the model of the wire drawing process, only the initial position RVE is selected. As a consequence, this fragment moves together with the material point over the deformation area. The following information is obtained from the solution for a single cell:

- The positions of grain boundaries in the process of deformation, and the values of deformation and stresses in the grains.

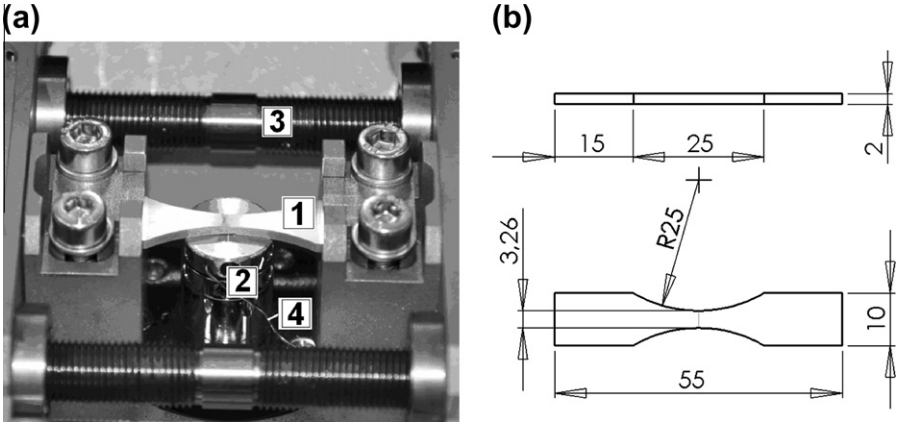

Fig. 2. (a) Photograph of the tensile/compression stage for the SEM: 1 – the sample, 2 – the heating device, 3 – the deformation device, 4 – the thermocouple, and a (b) drawing of the tensile sample.

Please cite this article in press as: Milenin A et al. The multi-scale physical and numerical modeling of fracture phenomena in the MgCa0.8 alloy. Comput Struct (2011), doi:10.1016/j.compstruc.2011.01.003

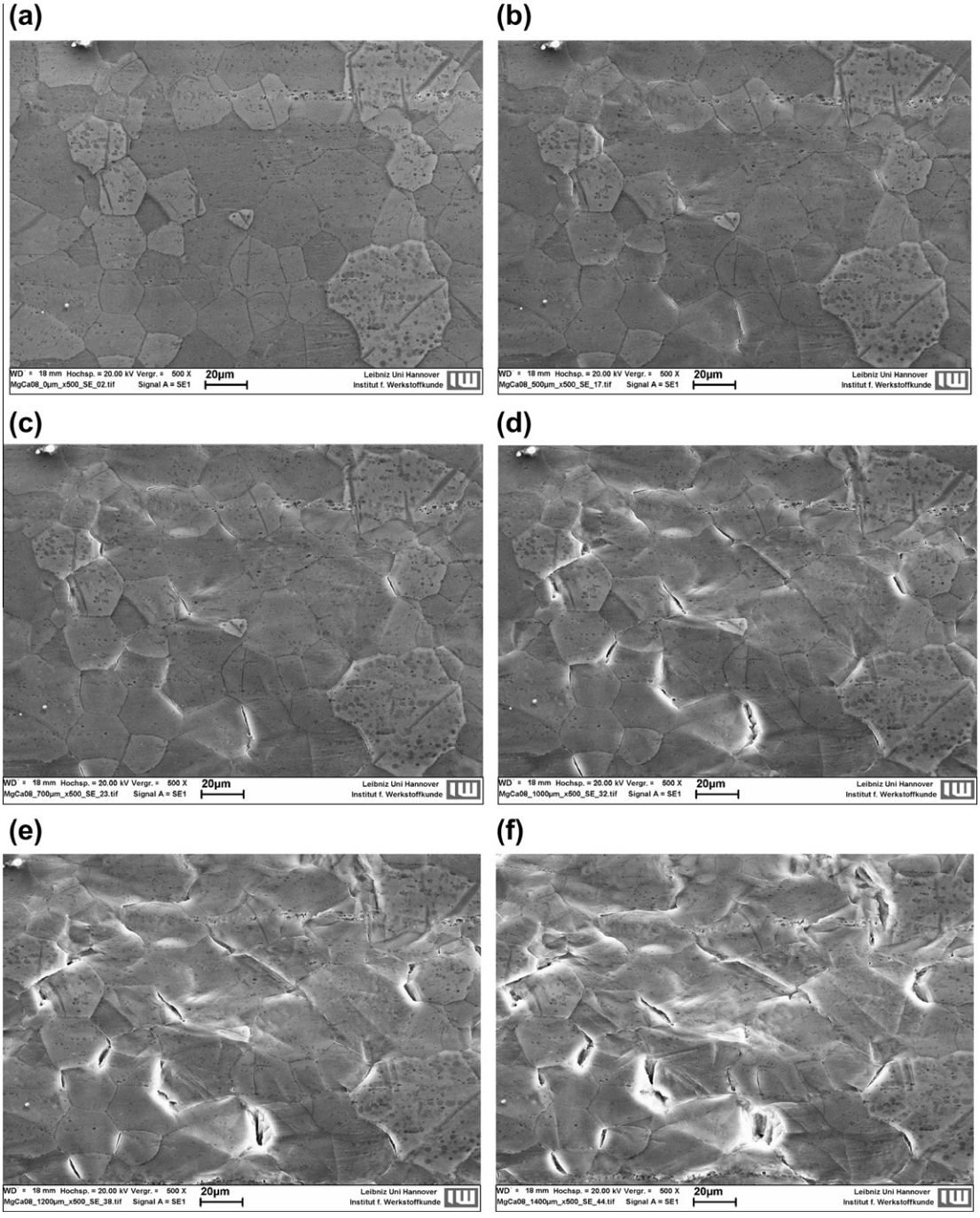

Fig. 3. Fracture mechanism at the micro-scale for MgCa0.8 at the center of the sample; (a) before tensile test, (b)–(f) during tensile test; the crosshead displacement is 0.5 mm (b), 0.7 mm (c), 1.0 mm (d), 1.2 mm (e) and 1.4 mm (f).

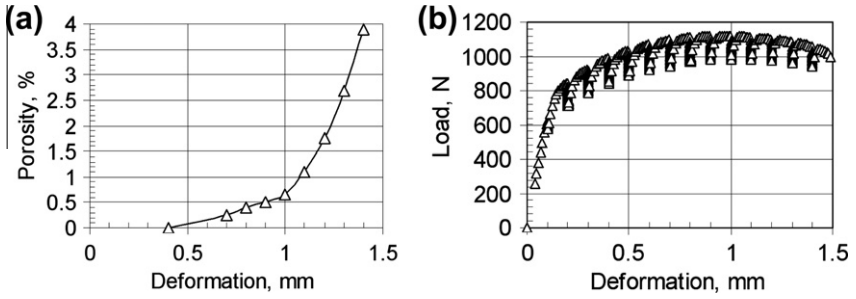

Fig. 4. (a) The dependence of the porosity on the deformation of the sample and (b) the load-deformation curve.

Please cite this article in press as: Milenin A et al. The multi-scale physical and numerical modeling of fracture phenomena in the MgCa0.8 alloy. Comput Struct (2011), doi:10.1016/j.compstruc.2011.01.003

- The value of the fracture parameter at the grain boundaries, crack initiation at the boundary and the corresponding stress relaxation in the grains.

These results are not used in the solution to the macro-scale problem. For this reason, there is no need to analyze the correlation between the size of the RVE and the criteria of homogenization, as it is reported elsewhere [39]. A unit cell side length of 103 × 76 μm is considered. In the case investigated here, the selection of the RVE size is connected to the area of the microstructure available for observation during the experiment.

The RVE is divided into elements with linear mechanical properties (Fig. 5). The model at the micro-scale includes the generation of the BEM mesh for a digital fragment of the microstructure and the numerical solutions at the micro-scale. The boundary conditions for the micro-scale model were either obtained from the solution of the boundary problem at the macro-scale or were taken directly from the experiment. During the simulation of tensile tests, the boundary conditions on the RVE were assigned in the form of displacements of the boundary RVE in the loading direction (axis x in Fig. 5). The extent of these displacements was determined on the basis of the measurement of the coordinates of the characteristic points of the fragment of microstructure during the process of its deformation. Thus, the transfer of strain (ε_x in Fig. 5) in the RVE was accomplished. The stresses (σ_y in Fig. 5) perpendicular to the tensile direction were assigned. In the simulations of the tensile test, pure tension stress was assumed and the value of σ_y was set to zero. In the wire drawing simulation, the boundary conditions were taken from the solution to the macro-scale problem. In this case, the lengthwise deformation and the stress in the transverse direction were also considered. Thus, the value of σ_y is not zero. For simplification of the solution, in both cases the RVE position was selected to be at the center line of the wire. As a consequence, the shear components of the stress and strains tensors were equal to zero. The merit of this approach is the fact that the same procedure is used during the identification of the parameters of the model and in the subsequent calculations of the wire drawing process. It should be emphasized that in this case, the possibilities for the selection of the method of setting the boundary conditions, which are obtained from the experiment, are limited.

The solution of boundary problems at the micro-scale is based on a fundamental solution of elasticity theory obtained by Kelvin [33]. The formulas of Kelvin for a two-dimensional domain are written as follows:

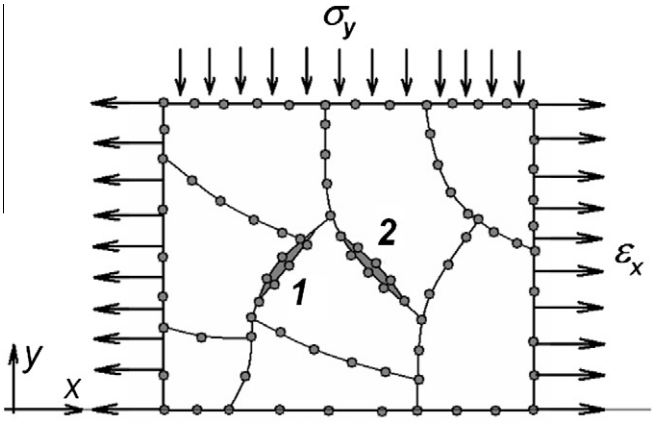

Fig. 5. The scheme for the model of the deformation process in the RVE: 1 and 2 are examples of cracks on grain boundaries; σ_y and ε_x are the boundary conditions taken from the macro-scale.

$$u_x = \frac{F_x(1+\nu)}{E}\left(g((3-4\nu) - x\frac{\partial g}{\partial x}\right) - \frac{F_y y(1+\nu)}{E}\frac{\partial g}{\partial x}, \tag{2}$$

$$u_y = \frac{F_y(1+\nu)}{E}\left(g(3-4\nu) - y\frac{\partial g}{\partial y}\right) - \frac{F_x x(1+\nu)}{E}\frac{\partial g}{\partial y}, \tag{3}$$

$$\sigma_x = F_x\left(2(1-\nu)\frac{\partial g}{\partial x} - x\frac{\partial^2 g}{\partial x^2}\right) + F_y\left(2\nu\frac{\partial g}{\partial y} - y\frac{\partial^2 g}{\partial x^2}\right), \tag{4}$$

$$\sigma_y = F_y\left(2(1-\nu)\frac{\partial g}{\partial y} - y\frac{\partial^2 g}{\partial y^2}\right) + F_x\left(2\nu\frac{\partial g}{\partial x} - x\frac{\partial^2 g}{\partial y^2}\right), \tag{5}$$

$$\sigma_{xy} = F_x\left((1-2\nu)\frac{\partial g}{\partial y} - x\frac{\partial^2 g}{\partial x^2}\right) - F_y\left((1-2\nu)\frac{\partial g}{\partial x} - y\frac{\partial^2 g}{\partial x \partial y}\right), \tag{6}$$

$$g(x,y) = -\frac{1}{4\pi(1-\nu)}\ln\sqrt{(x^2+y^2)}, \tag{7}$$

where F_x and F_y are components of the loads that are applied to the linear elastic material, u_x and u_y are the displacements in the x- and y-directions, and σ_x, σ_y, and σ_{xy} are the stresses due to the load F, E is the elastic–plastic modulus of the material or the Young's modulus in the elastic zone and ν is the Poisson's ratio of the material.

In the plastic deformation range, the material is considered to be incompressible, i.e. $\nu = 0.5$. To calculate the coefficients of the system of equations, the Castigliano theorem is used:

$$\int_S (t_n \upsilon_n + t_s \upsilon_s) dS = \int_S (\tau_n u_n + \tau_s u_s) dS, \tag{8}$$

where S is the surface of contact, t_n and t_s are the normal and shear stresses, u_n and u_s are the displacements at the boundary (in the boundary elements) and τ_n, τ_s, υ_n, and υ_s are the control solutions at the boundary determined on the basis of Eqs. (2)–(7).

A linear approximation of the displacements and stresses was used. The elastic–plastic modulus of the material for each grain was determined according to the following equation:

$$E = \frac{\sigma_i(\bar{\varepsilon}_i)}{\bar{\varepsilon}_i}, \tag{9}$$

where $\bar{\varepsilon}_i$ is the mean equivalent strain in the grain, and $\sigma_i(\bar{\varepsilon}_i)$ is the stress-strain relationship for the material (1).

To determine the value of $\bar{\varepsilon}_i$ from the geometric model of the grain, the central point of each grain is added. The displacement of this point is determined via the averaging of the values of displacements in the nodes of the boundary elements. The triangle, shown in Fig. 6, is examined for each boundary element. Based on the formulas for the simplex finite element, the deformations of each triangle were determined by the following equations:

$$\varepsilon_x = \frac{\partial u_x}{\partial x} = u_{xi}\frac{\partial N_i}{\partial x} + u_{xj}\frac{\partial N_j}{\partial x} + u_{xk}\frac{\partial N_k}{\partial x}, \tag{10}$$

$$\varepsilon_y = \frac{\partial u_y}{\partial y} = u_{yi}\frac{\partial N_i}{\partial y} + u_{yj}\frac{\partial N_j}{\partial y} + u_{yk}\frac{\partial N_k}{\partial y}, \tag{11}$$

$$\varepsilon_{xy} = \frac{1}{2}\left(\frac{\partial u_x}{\partial y} + \frac{\partial u_y}{\partial x}\right) = \frac{1}{2}\left(u_{xi}\frac{\partial N_i}{\partial y} + u_{xj}\frac{\partial N_j}{\partial y} + u_{xk}\frac{\partial N_k}{\partial y} + u_{yi}\frac{\partial N_i}{\partial x} + u_{yj}\frac{\partial N_j}{\partial x} + u_{yk}\frac{\partial N_k}{\partial x}\right), \tag{12}$$

$$\varepsilon_i = \frac{\sqrt{2}}{3}\sqrt{(\varepsilon_{xx} - \varepsilon_{yy})^2 + \varepsilon_{yy}^2 + \varepsilon_{xx}^2 + 6\varepsilon_{xy}^2}, \tag{13}$$

Please cite this article in press as: Milenin A et al. The multi-scale physical and numerical modeling of fracture phenomena in the MgCa0.8 alloy. Comput Struct (2011), doi:10.1016/j.compstruc.2011.01.003

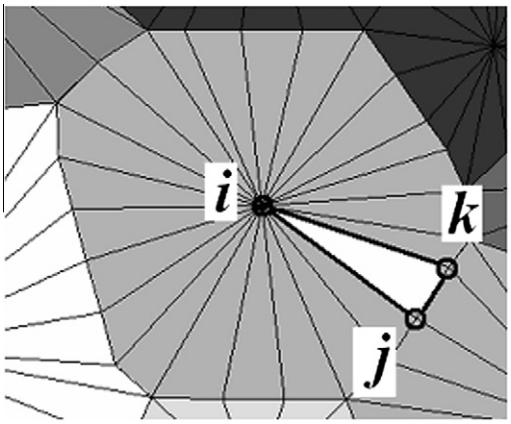

Fig. 6. The scheme for the strain calculation algorithm in the BEM model of the grain.

where N_i, N_j, and N_k are the shape functions of the triangle simplex element.

In the next stage, these values are averaged for each domain (grain) using the following formula:

$$\bar{\varepsilon}_i = \frac{\sum_{e=1}^{n} \varepsilon_{ie} A_e}{\sum_{e=1}^{n} A_e}, \tag{14}$$

where A_e is the area of the triangle simplex element e and ε_{ie} is the effective strain in the triangle simplex element e.

Adding the connection between grains and the probability of cracking at the grain boundaries, the following boundary conditions are introduced:

$$\sigma_s^{[1]}(x_q, y_q) = \sigma_s^{[2]}(x_q, y_q), \tag{15}$$

$$\sigma_n^{[1]}(x_q, y_q) = \sigma_n^{[2]}(x_q, y_q), \tag{16}$$

$$u_s^{[1]}(x_q, y_q) = -u_s^{[2]}(x_q, y_q), \tag{17}$$

$$u_n^{[1]}(x_q, y_q) = -u_n^{[2]}(x_q, y_q), \tag{18}$$

where $\sigma_s^{[1]}(x_q, y_q)$ and $\sigma_n^{[1]}(x_q, y_q)$ are the shear and normal stresses in the boundary elements of the first grain at the point (x_q, y_q) (the center of the boundary element) from the side of grain 1, $\sigma_s^{[2]}(x_q, y_q)$ and $\sigma_n^{[2]}(x_q, y_q)$ are the shear and normal stresses in the boundary elements of the second grain at the point (x_q, y_q) from the side of grain 2. A similar notation was used for displacements.

For the simulation of cracking along the boundary between elements 1 and 2, Eqs. (15)–(18) are excluded from system of algebraic equations (8), and the condition that $\sigma_s^{[1]} = \sigma_s^{[2]} = \sigma_n^{[1]} = \sigma_n^{[2]} = 0$ is introduced.

The proposed criteria of crack initiation are based on the theory by L. M. Kaczanov and Y. N. Rabotnov [40]. This theory was successfully used in another study [12] for the modeling of grain boundary cracking in the case of the deformation of polycrystals that fracture at the grain boundaries. This model was modified to describe the crack initiation at the grain boundary:

$$D = \int_0^{\tau} \dot{D} d\tau = 1, \tag{19}$$

$$\dot{D} = b_1 \left(\frac{\sigma_{eq}}{E}\right)^{b_2} (1 - D)^{b_3}, \tag{20}$$

$$\sigma_{eq} = \sqrt{\sigma_n^2 + b_0 \sigma_S^2}, \tag{21}$$

where D is the damage parameter, E is the Young's modulus, σ_n is the tensile (positive) component of the normal stress at the boundary between two grains, σ_s is the shear stress at the boundary between two grains and $b_0 - b_3$ are the empirical coefficients. In a previous work [12], a value of 0.4 was proposed for b_0.

In the model developed here, crack initiation is allowed only for the internal boundaries. The outer boundaries of the domains were assigned to boundary conditions, and in spite of a possible fulfillment of the condition, these boundaries cannot be destroyed.

The process of deformation is divided into small increments. Only one element of the boundary can be divided into layers in each stage of loading. Thus, sequential crack opening is simulated. The boundary elements, which correspond to the opened crack, are deformed as free surfaces. Because the stresses on these surfaces are equal to zero, the value of D on them does not increase further. The case corresponding to the possible convergence of the boundaries of cracks was not examined because it was of no practical interest to this study.

4.2. Determination of the empirical parameters of the fracture model at the micro-scale

The boundary conditions for the fracture modeling in tensile tests were taken directly from the experiment as the strain in the longitudinal direction (ε_x in Fig. 5) of the analyzed microstructure. The stress in the perpendicular direction (σ_y in Fig. 5) was assumed to be zero. The BEM model and the original fragment of the microstructure are shown in Fig. 7.

The results for the two-stage tensile test were analyzed. The total deformation (displacements of the crossheads) was 0.5 mm and 0.7 mm, which corresponds to a 7.810 μm and 10.93 μm RVE deformation, respectively. The results for the 0.5 mm deformation were used to determine the empirical coefficients in equation (20). The results for the 0.7 mm deformation were used to validate the model. The following objective function was used to determine $b_1 - b_3$:

$$\delta = \sum_{e=1}^{Ne} \left(D_{calc}^{[e]} - 1\right)^2, \tag{22}$$

where e is the number of the given boundary that fractured in the experiment, N_e is the number of boundaries that fractured at the given moment of deformation and $D_{calc}^{[e]}$ is the calculated value of D in the cracked boundary (it must be equal 1.0 at the moment of cracking). The minimum of the objective function is reached by a variation of the coefficients $b_1 - b_3$. The following values of the coefficients were obtained: $b_1 = 0.0197$, $b_2 = 0.430$, $b_3 = 0.860$ ($b_0 = 0.4$ [12]). The results of the simulation obtained for these values of coefficients are shown in Figs. 8 and 9.

The results of the calculations for the deformation of 0.7 mm are shown in Figs. 10 and 11. The comparison of the calculated and experimental crack localization is shown in Fig. 10. A good qualitative agreement with the crack predictions is obtained. The locations of the crack initiation coincided with the experimental result very well (Fig. 10). On the other hand, this agreement is worse for the proportion of the distance to the boundary of the domain (e.g., the upper crack in Fig. 10(b) is not observed in the calculations).

The distribution of normal stresses along the grain boundaries is shown in Fig. 9(b) and Fig. 11(b). The auxiliary grid of finite elements is used to visualize the stress distribution. At the central point of the domains, the stress is equal to zero. The distribution of parameter D along the grain boundaries is shown in Fig. 9(a) and Fig. 11(a). Because it results from data shown in Fig. 9(b) and Fig. 11(b), the normal stress at the grain boundaries increases with increased deformation. When the crack propagates, the stress on the crack edge becomes zero. This leads to the unloading of the grains, which is visible from the strain distribution in Fig. 8(a) and

Please cite this article in press as: Milenin A et al. The multi-scale physical and numerical modeling of fracture phenomena in the MgCa0.8 alloy. Comput Struct (2011), doi:10.1016/j.compstruc.2011.01.003

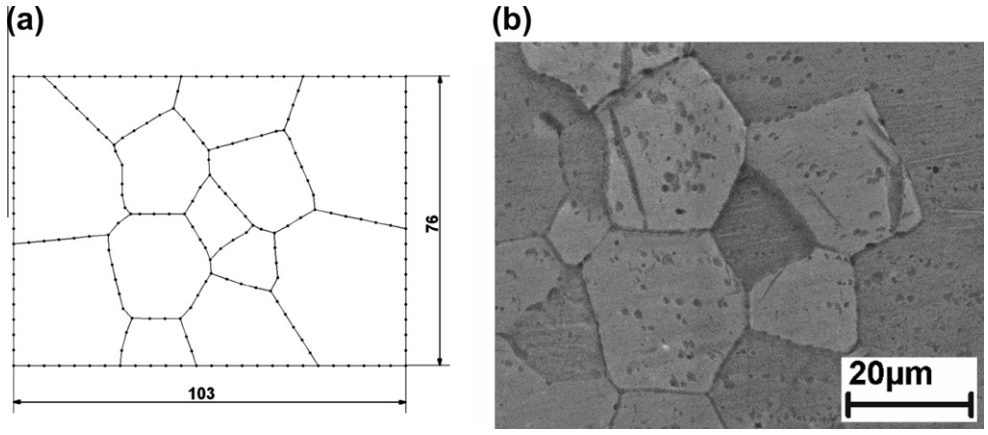

Fig. 7. (a) The BEM model of the fragment of the initial microstructure in (b).

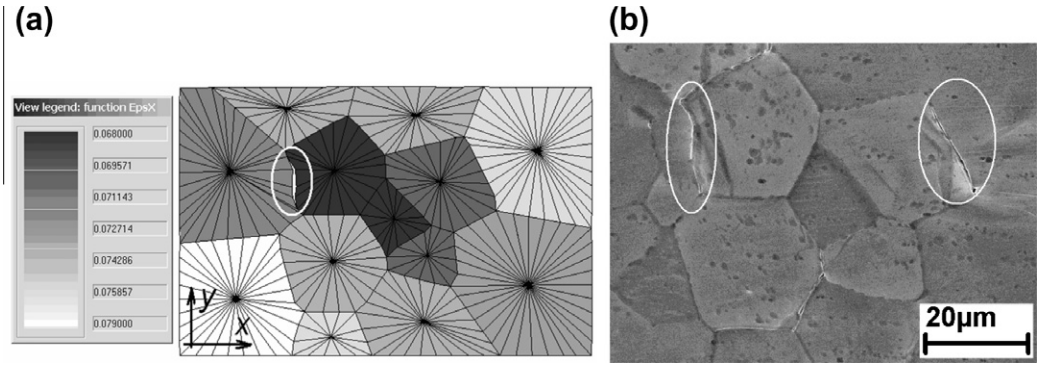

Fig. 8. (a) The BEM model and calculated longitudinal strain ε_x in grains for the fragment of the microstructure in (b) after a 0.5 mm deformation of the sample in the micro-chamber for the SEM.

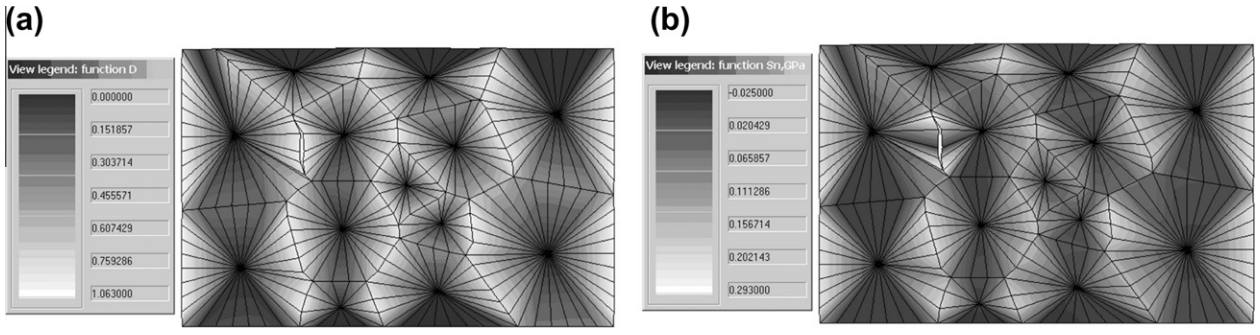

Fig. 9. (a) The calculated distribution of D (b) the normal stress σ_n in GPa along the grain boundaries for the fragment of the microstructure after a 0.5 mm deformation of the sample.

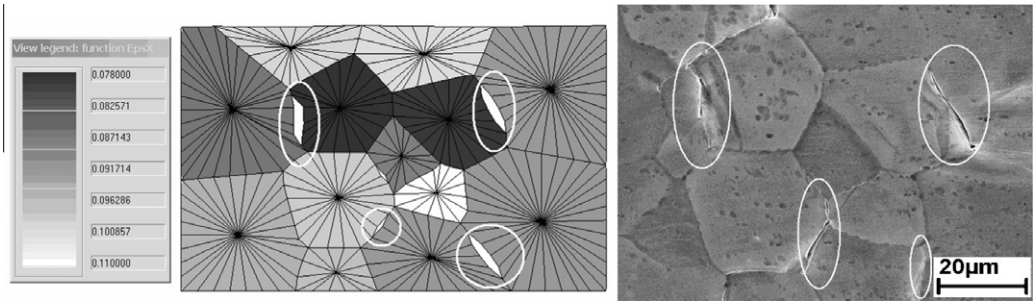

Fig. 10. (a) The BEM model and calculated longitudinal strain ε_x in the grains for the fragment of the microstructure in (b) after a 0.7 mm deformation of the sample in the SEM micro-chamber.

Please cite this article in press as: Milenin A et al. The multi-scale physical and numerical modeling of fracture phenomena in the MgCa0.8 alloy. Comput Struct (2011), doi:10.1016/j.compstruc.2011.01.003

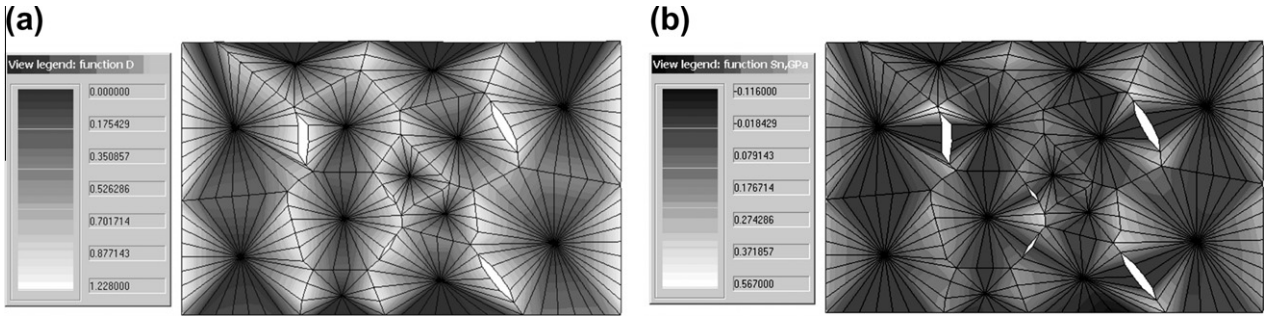

Fig. 11. (a) The calculated distribution of D (b) the normal stress σ_n in GPa along the grain boundaries for the fragment of the microstructure after a 0.7 mm deformation of the sample.

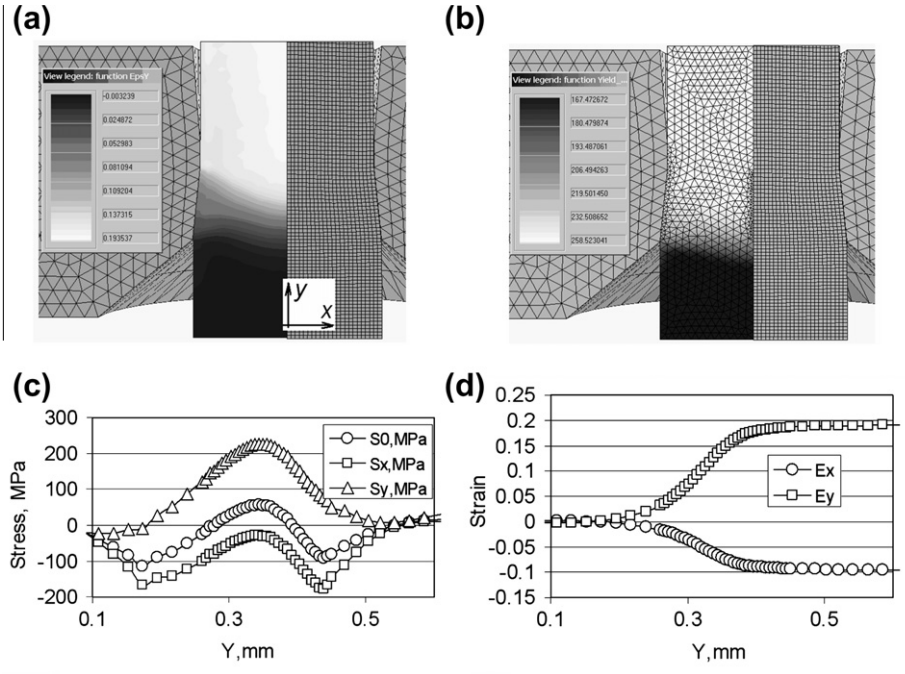

Fig. 12. The results of the wire drawing simulation for variant 1: (a) the distribution of the strain ε_y; (b) the distribution of the yield stress in GPa; (c) the values of the stresses on the centerline of the wire (y-axis); (d) the values of the strains on the centerline of the wire.

Fig. 10(a). Smaller values of the longitudinal deformation correspond to a darker color in these figures.

4.3. A model of wire drawing as a macro-scale and multi-scale conception

The proposed model at the micro-scale is implemented in the FEM code developed by the authors [38]. This code is dedicated to the modeling of wire drawing processes. In this FEM model, a boundary problem takes into account plastic deformation, heat transfer, and wire heating due to deformation and friction. The solution to the boundary problem is obtained by using the variation principle of the rigid-plastic theory:

$$J = \int_V \int_0^{\xi_i} \sigma_i(\varepsilon_i, \xi_i, t) d\xi_i dV + \int_V \sigma_0 \xi_0 dV - \int_S \sigma_\tau v_\tau dS, \tag{23}$$

where ξ_i is the strain rate intensity, ε_i is the strain intensity, t is the temperature, V is the volume, σ_0 is the mean stress, ξ_0 is the volumetric strain rate; S is the contact area between the alloy and the die, σ_τ is the friction stress and v_τ is the alloy slip velocity along the surface of die.

The friction stress is determined according to the following equation:

$$\sigma_\tau = f_{tr} \frac{\sigma_i}{\sqrt{3}} \left(1 - \exp\left(-\frac{1.25\sigma_n}{\sigma_i}\right)\right), \tag{24}$$

where f_{tr} is the friction coefficient and σ_n is the normal stress on contact between the alloy and the crosshead.

The components of the deformation tensor ε_{ij} are calculated by integration of each strain rate tensor component along flow lines. Implementation in the FEM code of the fracture model was performed for the central line of the wire. Boundary conditions for the task at the micro-scale are obtained from the solution at the macro-scale. The deformation in the direction of wire drawing and the vertical stress are selected as the parameters to be analyzed. The applied method is different from the approaches utilized for the identification of the model of destruction by the presence of the vertically compressive stress (Fig. 5), but the same representation of the microstructure is used in analysis presented here.

Please cite this article in press as: Milenin A et al. The multi-scale physical and numerical modeling of fracture phenomena in the MgCa0.8 alloy. Comput Struct (2011), doi:10.1016/j.compstruc.2011.01.003

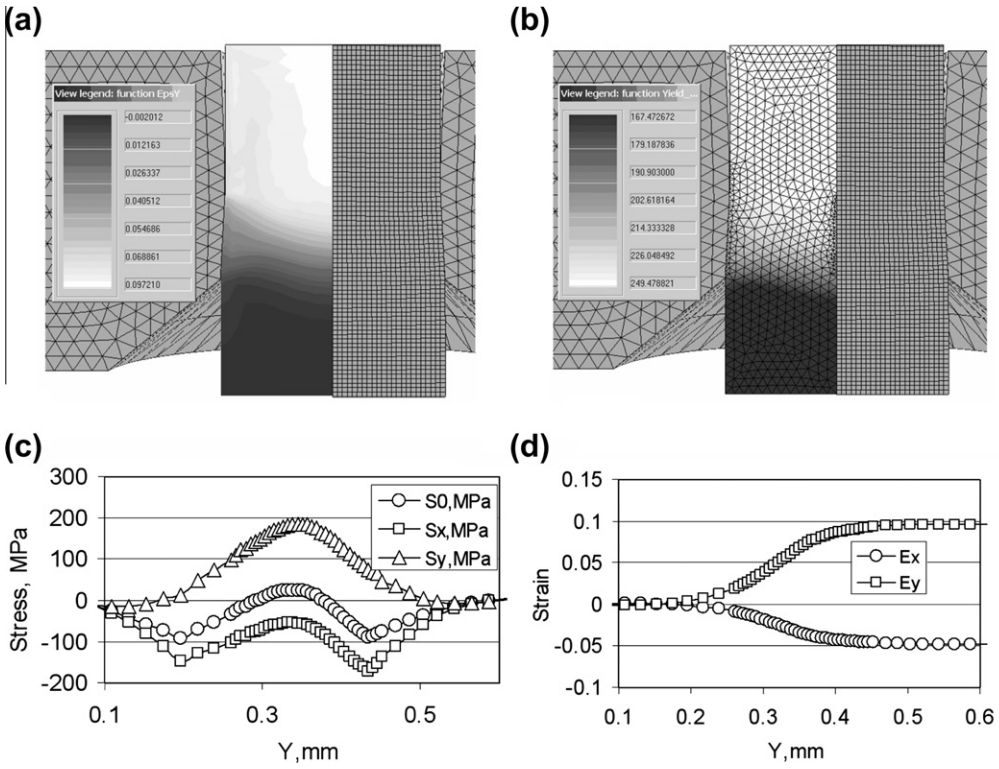

Fig. 13. Results of the wire drawing simulation for variant 2: (a) the distribution of the strain ε_y; (b) the distribution of the yield stress in GPa; (c) the values of the stresses on the centerline of the wire (y-axis); (d) the values of the strains on the centerline of the wire.

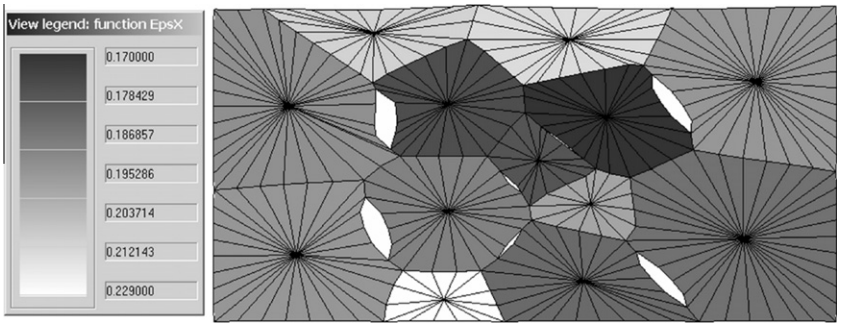

Fig. 14. The BEM model of the RVE for centerline of the wire and the calculated longitudinal strain in grains for the fragment of the microstructure after drawing according to variant 1.

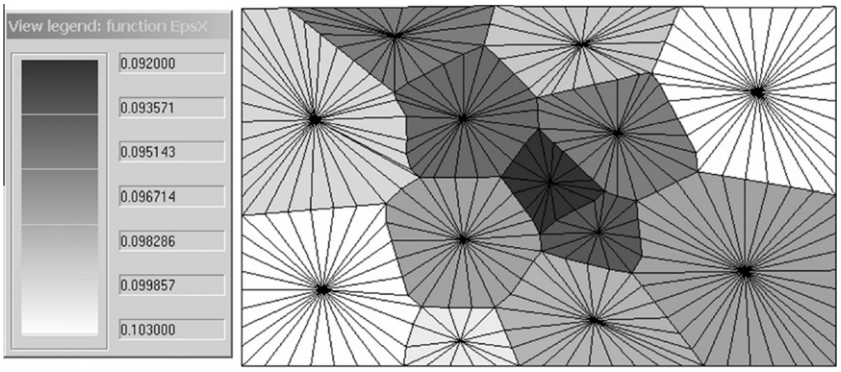

Fig. 15. The BEM model of the RVE for centerline of the wire and the calculated longitudinal strain in grains for the fragment of the microstructure after drawing according to variant 2.

Please cite this article in press as: Milenin A et al. The multi-scale physical and numerical modeling of fracture phenomena in the MgCa0.8 alloy. Comput Struct (2011), doi:10.1016/j.compstruc.2011.01.003

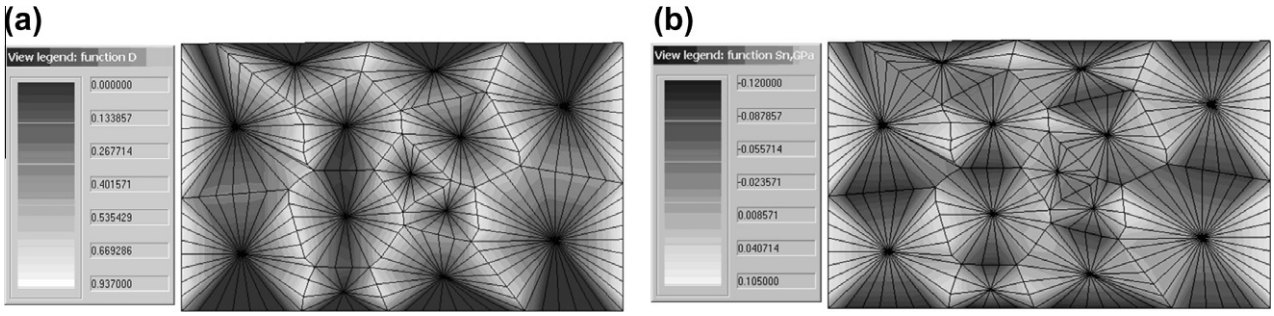

Fig. 16. (a) The calculated distribution of D and (b) the normal stress σ_n in GPa along grain boundaries for the fragment of the microstructure after drawing according to variant 2.

5. Results and discussion

The calculations for two versions of wire drawing of the MgCa0.8 alloy were analyzed with the aid of the model developed in this study. The general data are as follows: the speed of drawing is 0.05 m/s, the initial diameter of the wire is 0.5 mm and the coefficient of friction is 0.03. The remaining data are as follows:

Variant 1: the wire diameter after drawing is 0.46 mm, and the semi angle of the die is 6°.
Variant 2: the wire diameter after drawing is 0.48 mm, and the semi angle of the die is 4°.

The results of the wire drawing simulation at the macro-scale are presented in Figs. 12(variant 1) and 13(variant 1). The distribution of the yield stress (Figs. 12 and 13(b)) is shown together with the finite elements mesh. The mesh is finer on the centerline of wire. The distributions of the components of the stress and strain tensors along the centerline of the wire are shown in Figs. 12 and 13(c) and (d). The strain ε_x distribution and the vertical stress σ_y are used as the boundary conditions for the RVE. The results that were obtained with the aid of the model at the micro-scale show that, in the first variant, microscopic cracks might occur at the grain boundaries (Fig. 14). However, variant 2 permits one to obtain a state in the wire that is close to the optimum strain state and to maximally use the possibilities of annealing for restoring the plasticity (Fig. 15). In this case, the state of the metal corresponds approximately to experiment number 3 in Table 2. This results from the value of parameter D, which approaches a limiting value (Fig. 16(a)). The value of deformation in the direction of wire drawing in this case is 0.1 (Fig. 15(a)).

The addition of compressive stresses leads to increases in the permissible metal deformation. Fig. 16(b) shows the distribution of normal stresses at the grain boundaries. As a result, the effects of the vertical compressive stresses in the domain and the maximum tensile stresses on the grain boundaries are reduced. According to equation (20), an increase in the plasticity of the material is reached. In pure tension (Fig. 8(a)), the initiation of fracture is observed at a substantially smaller strain (0.079).

The essential influence of the stress state on the plasticity is well-known [9]. Further improvement of the represented model will be achieved by applying it to the identification of experimental data, which are obtained for the samples deformed in different stress states.

6. Conclusions

Experimental studies showed that the state that precedes the appearance of microscopic cracks at the grain boundaries is the optimum state of the metal after deformation but before annealing. The prediction of this state for wire drawing requires the creation of a multi-scale model.

Thus, a new multi-scale model of the fracture phenomena in the MgCa0.8 alloy is proposed in this paper. The conception of a simulation of the fracture is based on the boundary elements method and on the results of physical modeling at the micro-scale level.

The following phenomena are predicted by the mathematical model of fracture at the micro-scale: stresses and strains at the grains before grain boundary cracking, stress relaxation along the grain after cracking, the shape and moment of initiation of micro cracks, fracture phenomena at the macro-scale.

The proposed model is implemented in the authors' FEM code, which is dedicated to modeling wire drawing processes. The computer program developed in this study enables predictions and observations of discontinuity in grains boundaries during deformation.

Acknowledgment

Financial assistance from the Ministry of Science and high Education of Poland, project no. 4131/B/T02/2009/37, is acknowledged.

References

[1] Heublein B, Rohde R, Niemeyer M, Kaese V, Hartung W, Röcken C, Hausdorf G, Haverich A. Degradation of Magnesium Alloys: A new principle in cardiovascular implant technology, Paper TCT-69, 11. Annual Symposium "Transcatheter Cardiovascular Therapeutics", The American Journal of Cardiology, Expcerpta Media Inc., New York; 1999.
[2] Haferkamp H, Kaese V, Niemeyer M, Phillip K, Phan-Tan T, Heublein B, et al. Exploration of magnesium alloys as new material for implantation. Mat-wiss.u 2001;32:116–20.
[3] Thomann M, Krause Ch, Bormann D, von der Hoh N, Windhagen H, Meyer-Lindenberg A. Comparison of the resorbable magnesium alloys LAE442 and MgCa0.8 concerning their mechanical properties, their progress of degradation and the bone-implant-contact after 12 months implantation duration in a rabbit model. Mat.-wiss. u. Werkstofftech 2009;40(1–2):82–7.
[4] Odawa N, Shiomi M, Osakada K. Forming limit of magnesium alloy at elevated temperatures for precision forming. International Journal of Machine Tools and Manufacture 2002;42:607–14.
[5] Yoshida K. Cold drawing of magnesium alloy wire and fabrication of microscrews. Steel Grips 2004;2:199–202.
[6] Bach Fr-W, Hassel T, Golovko AN. The Influence of the chemical composition and extrusion parameters on the mechanical properties of thin-walled tubes made of magnesium-calcium alloys, Suczasni problemy metalurgii Naukovi visti. Systemni technologii 2005;8:379–84.
[7] Bach Fr-W, Milenin A, Kucharski R, Borman D, Kustra P. Modelowanie za pomocą MES procesu ciągnienia drutów ze stopu magnezu wykorzystywanych w chirurgii. Hutnik-Wiadomosci Hutnicze 2007;74:8–11. in Polish.
[8] Kustra P, Milenin A, Schaper M, Grydin O. Multiscale modeling and interpretation of tensile test of magnesium alloy in microchamber for the SEM. Computer Methods in Materials Science 2009;9:207–14.
[9] Bao Y, Wierzbicki T. On fracture locus in the equivalent strain and stress triaxility space. International Journal of Mechanical Sciences 2004;46:81–98.
[10] Allix O, Leveque D, Perret L. Identification and forecast of delamination in composite laminates by an interlaminar interface model. Composites Science and Technology 1998;58:671–8.

Please cite this article in press as: Milenin A et al. The multi-scale physical and numerical modeling of fracture phenomena in the MgCa0.8 alloy. Comput Struct (2011), doi:10.1016/j.compstruc.2011.01.003

[11] Rabczuk T, Zi G, Bordas S. A geometrically non-linear three-dimensional cohesive crack method for reinforced concrete structures. Engineering Fracture Mechanics 2008;75(16):4740–58.
[12] Diard O, Leclercq S, Rousselier G, Cailletaud G. Distribution of normal stress at grain boundaries in multicrystals: application to an intergranular damage modeling. Computational Materials Science 2002;18:73–84.
[13] Grydin O, Schaper M, Bach Fr-W. Analysis of microstructure evolution during cold deformation of air-hardening steel LH800. Proc. of the EPD Congress 2009, TMS; 2009. p. 91-100.
[14] Schaper M, Grydin O. Experimentelle Untersuchungen der Mikrostruktur-entwicklung und mechanischen Eigenschaften von Metallen mittels Zug/Druck/Biegemodul im Rasterelektronenmikroskop. Proc. of 43th Metallographie Tagung 2009:139–44. in German.
[15] Milenin A, Kustra P. The multiscale FEM simulation of wire fracture phenomena during drawing of Mg alloy. Steel Research International 2008;79:717–22.
[16] Kerfriden P, Allix O, Gosselet P. A three-scale domain decomposition method for the 3D analysis of debonding in laminates. Computational Mechanics 2009;44(3):343–62.
[17] Ladeveze P, Moes N, Douchin B. Constitutive relation terror estimators for (visco)plastic finite element analysis with softening. Computer Methods in Applied Mechanics and Engineering 1999;176:247–64.
[18] Karihaloo BL, Xiao QZ. Modelling of stationary and growing cracks in FE framework without remeshing: a state-of-the-art review. Computers and Structures 2003;81(3):119–29.
[19] Belytschko T, Gracie R, Ventura G, Ogata S, Umeno Y, Kohyama M, et al. A review of extended/generalized finite element methods for material modeling. Proceedings of the 7th World Congress of Computational Mechanics on Computational Bridging of Length Scales in Complex Materials 2006;20:21.
[20] Bordas S, Nguyen PV, Dunant C, Guidoum A, Nguyen-Dang H. An extend finite element library. International for Numerical Methods in Engineering 2007;71(6):703–32.
[21] Chahine E, Laborde P, Renard Y. Spider-xfem, an extended finite element variant for partially unknown crack-tip displacement. European of Computational Mechanics 2008;15(5–7):625–36.
[22] Menk A, Bordas S. Numerically determined enrichment functions for the exted finite element method and applications to bi-material anisotropic fracture and polycrystals. International for Numerical Methods in Engineering 2010;83:805–28.
[23] Xiao QZ, Karihaloo BL. Improving the accuracy of XFEM crack tip fields using higher order quadrature and statically admissible stress recovery. International Journal for Numerical Methods in Engineering 2006;66(9):1378–410.
[24] Xuan ZC, Lassila T, Rozza G, Quarteroni A. On computing upper and lower bounds on the outputs of linear elasticity problems approximated by the smoothed finite element method. International Journal for Numerical Methods in Engineering 2010;83(2):174–95.
[25] Nguyen-Xuan H, Rabczuk T, Bordas S, Debongnie JF. A smoothed finite element method for plate analysis. Computer Methods in Applied Mechanics and Engineering 2008;197(13–16):1184–203.
[26] Nguyen-Xuan H, Bordas S, Nguyen-Dang H. Smooth finite element methods: convergence accuracy and properties. International Journal for Numerical Methods in Engineering 2008;74(2):175–208.
[27] Nguyen-Thanh N, Rabczuk T, Nguyen-Xuan H, Bordas S. An alternative alpha finite element method (A alpha FEM) for free and forced structural vibration using triangular meshes. Computational and Applied Mathematics 2010;233(9):2112–35.
[28] Nguyen VP, Rabczuk T, Bordas S. Meshless methods: a review and computer implementation aspects. Mathematics and Computers in Simulation 2008;79(3):763–813.
[29] Rabczuk T, Bordas S, Goangseup Zi. On three-dimensional modelling of crack growth using partition of unity methods. Computers and Structures 2010;88(23–24):1391–411.
[30] Rabczuk T, Bordas S, Zi G. A three-dimensional meshfree method for continuous multiple-crack initiation propagation and junction in statics and dynamics. Computational Mechanics 2007;40(3):473–95.
[31] Bordas S, Rabczuk T, Zi G. Three-dimensional crack initiation propagation branching and junction in non-linear materials by an extended meshfree method without asymptotic enrichment. Engineering Fracture Mechanics 2008;75(5):943–60.
[32] Rabczuk T, Bezensek B, Bordas S, Application of Extended Element-Free Galerkin Method to Multiple Flaws Under Brittle Fracture Conditions, Proceedings of the ASME Pressure Vessels and Piping Conference 2008, vol.6. 2009. p. 1658.
[33] Crouch SL, Starfield AM. Boundary element methods in solid mechanics. London, Boston, Sydney: GEORGE ALLEN & UNWIN; 1983.
[34] Richardson JD, Cruse TA. Nonsingular BEM for fracture modeling. Computers and Structures 1998;66:695–703.
[35] Milenin A. Comparative analysis of boundary and finite element method possibilities in simulation of metal working processes. Russian metallurgy, Metally ISSN 0036-0295, Allerton Press, London, ROYAUME-UNI, 2, 1997. p. 64-71.
[36] Milenin A. A plastic-deformation simulation of two-phase materials by the boundary-elements method. Metallofizika I Novejshie Tekhnologii. 1995;17:46–52.
[37] Szeliga D, Pietrzyk M. Testing of the inverse software for identification of rheological models of materials subjected to plastic deformation. Archives of Civil and Mechanical Engineering 2007;7(1):35–52.
[38] Milenin A. Program komputerowy Drawing2d-narzędzie do analizy procesów technologicznych ciągnienia wielostopniowego. Hutnik-Wiadomości Hutnicze 2005;72:100–4. in Polish.
[39] Gitman IM, Askes H, Aifantis EC. The Representative Volume Size in Static and Dynamic Micro-Macro Transitions. International Journal of Fracture 2005. 135:L3-135:L9.
[40] Rabotnov YN. Creep problems in structural members. North-Holland 1969.

Please cite this article in press as: Milenin A et al. The multi-scale physical and numerical modeling of fracture phenomena in the MgCa0.8 alloy. Comput Struct (2011), doi:10.1016/j.compstruc.2011.01.003